Reprinted from MONTHLY WEATHER REVIEW, Vol. 119, No. 3, March 1991
American Meteorological Society

A Typhoon Observed with the MU Radar

TORU SATO

Department of Electrical Engineering II, Kyoto University, Kyoto, Japan

NAOKI AO, MAMORU YAMAMOTO, SHOICHIRO FUKAO, TOSHITAKA TSUDA AND SUSUMU KATO

Radio Atmospheric Science Center, Kyoto University, Kyoto, Japan

(Manuscript received 16 April 1990, in final form 2 October 1990)

ABSTRACT

During the passage of Typhoon 8719 a 60-h continuous observation was made of the troposphere and the lower stratosphere with the MU (middle and upper atmosphere) radar. Height profiles of the wind velocity vector were measured every 2.5 min with a height resolution of 150 m. The typhoon struck Japan's main island on 17 October 1987, and passed within 100 km of the MU radar. A clear turning of the wind velocity associated with the typhoon was observed up to a height of around 18 km, while short-period wind fluctuations showed strong effects associated with the typhoon up to 24 km. Prominent waves with vertical wavelength of 2–4 km and apparent period of ~10 h were found throughout the observation period. The vertical hodograph analysis revealed that these waves propagate both upward and downward from around the layer of a temperature inversion, suggesting the generation of these waves from that layer.

1. Introduction

While most studies on tropical cyclones have been made from a viewpoint of disaster prevention, they have another aspect of being ideal test cases for the study of atmospheric dynamics. Recent advances in measurement techniques have enabled detailed observations of three-dimensional structures of the tropical cyclones.

Among various types of tropical cyclones, the largest number of observational studies has been devoted to hurricanes. Many coordinated observations have been carried out using research aircraft that penetrate into the inner core (e.g., Jorgensen 1984a,b), and have substantially contributed to the establishment of the morphology of hurricanes. The accuracy of vertical motion measurements has been improved significantly by the use of inertial navigation equipment (Jorgensen et al. 1985). A noticeable improvement was made on the coverage of radar observations by development of airborne Doppler radars (Marks and Houze 1984, 1987). Omega dropwindsondes also have been introduced to complement the radar observations (Franklin et al. 1988).

In the Asian sector, the three-dimensional structure of typhoons has been intensively studied. A climatology of typhoons in their developing and mature stages has recently been developed based on a long history of routine aircraft observations (Weatherford and Gray 1988a,b). The decaying stage of typhoons has been studied in detail in Japan by various observation techniques including recent developments of single- (Sakakibara et al. 1985) and dual-Doppler radars (Ishihara et al. 1986). Heavy rainstorms and rainbands associated with typhoons, which cause serious damage, have been the major targets of these observations.

The MST (mesosphere–stratosphere–troposphere) radar technique has a unique capability of measuring the background air motion. It makes use of weak scattering of VHF or UHF radio waves from irregularities in the atmospheric index of refraction due to turbulence. Although the horizontal coverage of these radars is usually limited by a large antenna aperture, which is hard to steer to low elevation angles, they can observe above the tropopause height and motions in a clear sky continuously in time. The capability of MST radars in meteorological applications has been reviewed by Balsley and Gage (1980) and Larsen and Röttger (1982). The MST radars can be a powerful tool in observing the vertical structure of tropical cyclones.

The first observations of a typhoon using the MST radar technique was made with the MU (middle and upper atmosphere) radar at Shigaraki, Japan (34.9°N, 136.1°E), on 13–18 August 1983 (Kato et al. 1984). The MU radar was operational at that time with a partial system, roughly one-eighth the capability of the current system both in the antenna area and the output power. Also, the antenna beam was not steerable during observations, so that the observation was made with

Corresponding author address: Dr. Toru Sato, Dept. of Electrical Engineering II, Kyoto University, Kyoto 606, JAPAN.

one beam direction (10° east of zenith) only. Nevertheless, a clear vertical structure of the wind field associated with the typhoon was observed to about 12 km. Various gravity waves were also detected by the observation.

An ST (stratosphere–troposphere) radar, which is a smaller version of an MST radar, was constructed at Chung Li, Taiwan (Chao et al. 1986), and has been in successful operation since 1985. The Chung Li radar has an ideal location to study typhoons in their developing stage since it is on the middle of a typical course of typhoon. A short observation of the vector wind field accompanied with a typhoon has already been reported (Hung et al. 1988).

No close encounter of a typhoon to the MU radar in Japan had occurred since 1983 until Typhoon 8719 passed by at a distance of about 100 km from the radar on 17 October 1987, when the decaying stage of the typhoon was observed in detail. The MU radar was fully operational during the passage of the typhoon, and observations were made for about 60 h around the closest encounter. The three components of the wind vector were measured continuously for the entire height range of 1.5–24 km.

Here, the preliminary analysis results are reported. The basic results are first presented, such as the mean wind field associated with the typhoon and the background atmospheric conditions during the observation period. Then some of the prominent wave activity associated with the typhoon is examined.

2. Observational techniques

The MU radar is a 46.5-MHz monostatic Doppler radar with an active phased-array antenna 103 m in diameter and with 1-MW peak output power. The antenna beam direction can be steered to any direction within a zenith angle of 30°, and can be switched randomly from pulse-to-pulse. This fast steerability of the antenna beam enables measurement of the three components of the "instantaneous" wind vector derived from the line-of-sight Doppler velocity along different beam directions. Readers are referred to Fukao et al. (1985a,b) for details of the system.

The MU radar operated in two modes during the observation period: the troposphere mode with 1-μs single pulse, which observes a height region of 1.5–10 km, and the stratosphere mode with 16-element complementary codes with 1-μs subpulse width, which covers 5.4–24 km. These two modes are switched alternately every 75 s, so that the entire height region of 1.5–24 km can be covered in 2.5 min. Five beam directions: vertical and zenith angles 10° north, east, south, and west are observed with a range resolution of 150 m. The beam directions are switched every IPP (interpulse period) 400 μs in a cyclic manner.

The line-of-sight Doppler velocity and the echo power are determined by fitting a Gaussian curve to the observed echo power spectrum at each range gate (Yamamoto et al. 1988). The zonal wind velocity component is determined from the line-of-sight velocities of a pair of antenna beams pointing toward the east and west, and the meridional component from the north–south beam pair. The vertical component is directly determined using the vertically pointing antenna beam.

For tropospheric observations, where the signal-to-noise ratio is usually sufficiently high, the accuracy of the wind is determined by the magnitude of statistical fluctuations of the scattered echo, which is inversely proportional to the square root of the number of spectral averages. The magnitude of random errors in the horizontal and vertical wind velocity in the present case is estimated to be 0.7 m s^{-1} and 0.1 m s^{-1}, respectively, by numerical simulations (Yamamoto et al. 1988).

It should be noted that the vertical velocity below the freezing height (about 4 km in the present case) may be biased toward negative due to possible contaminations by precipitation echoes. Although the scattering cross section of raindrops at the wavelength of 6.4 m is much smaller compared to that for conventional weather radars, it is still comparable to the cross section of atmospheric turbulence. There is a series of successful studies to identify the secondary peak due to precipitation in the MU radar echo power spectra and to determine the drop-size distribution together with the background wind velocity (see Sato et al. 1990).

However, clear double-peaked Doppler spectra were not found during the present observation, partly due to strong turbulent motion in the lower atmosphere, which broadens the spectra and masks the secondary peaks. In such cases the estimated vertical velocity becomes a weighted mean of the vertical wind and the vertical precipitation velocity, the weight for which is the echo power of the two spectral components. Although the echo power of the atmospheric turbulence component is 10–20 dB larger than that of the precipitation component for most cases, where the error is less than 1 m s^{-1}, the precipitation component may have comparable or even larger echo power for an extreme case when a heavy rain falls through a region of weak turbulence.

3. Mean wind associated with Typhoon 8719

Typhoon 8719 was upgraded from a tropical depression on 11 October 1987 east of the Philippines. It evolved while proceeding northwestward, reaching its most mature stage with a central pressure of 975 mb and peak winds of 40 m s^{-1} on 15 October, 80 km east of Minami-Daitojima Island (Fig. 1). It then tracked northward, landed on Shikoku Island at 0000 JST 17 October, crossed the island, and finally landed

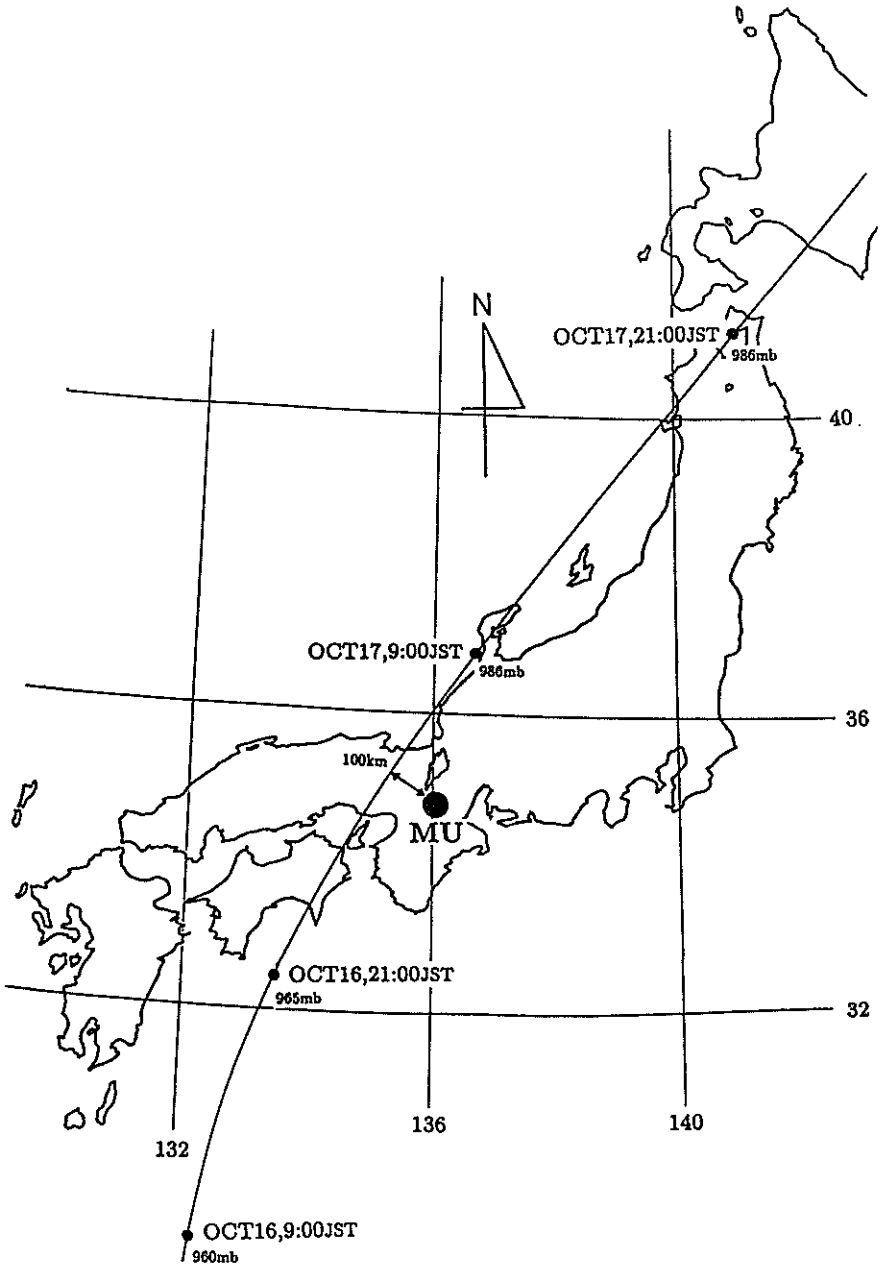

FIG. 1. Route of the center of Typhoon 8719.

on Honshu Island (mainland Japan) at 0400 JST. The central pressure at 0300 JST was 975 mb with peak winds of 30 m s^{-1}. The storm speeded up and further proceeded toward the north-northeast, until it decayed over the Sea of Japan at 0700 JST 17 October. The typhoon is estimated to have passed northwest of the MU radar at around 0500 JST 17 October with the minimum distance of about 100 km. Observations with the MU radar started at 2000 JST 15 October and continued for 60 h until 0800 JST 18 October. Figure 2 shows a time–height cross section of the horizontal wind velocity. A rotating wind field associated with the passage of the typhoon is clearly shown in the figure. The effect of the typhoon on the mean wind is observed up to about 18 km. Although the asymmetry in the wind speed about the time of passage is partly due to the relatively fast motion of the typhoon of about 13 m s^{-1} toward the northeast, it also shows that the typhoon was already decaying when it passed by the MU radar. This is consistent with the fact that the eye structure is evident in satellite pictures only until around 0300 JST 17 October.

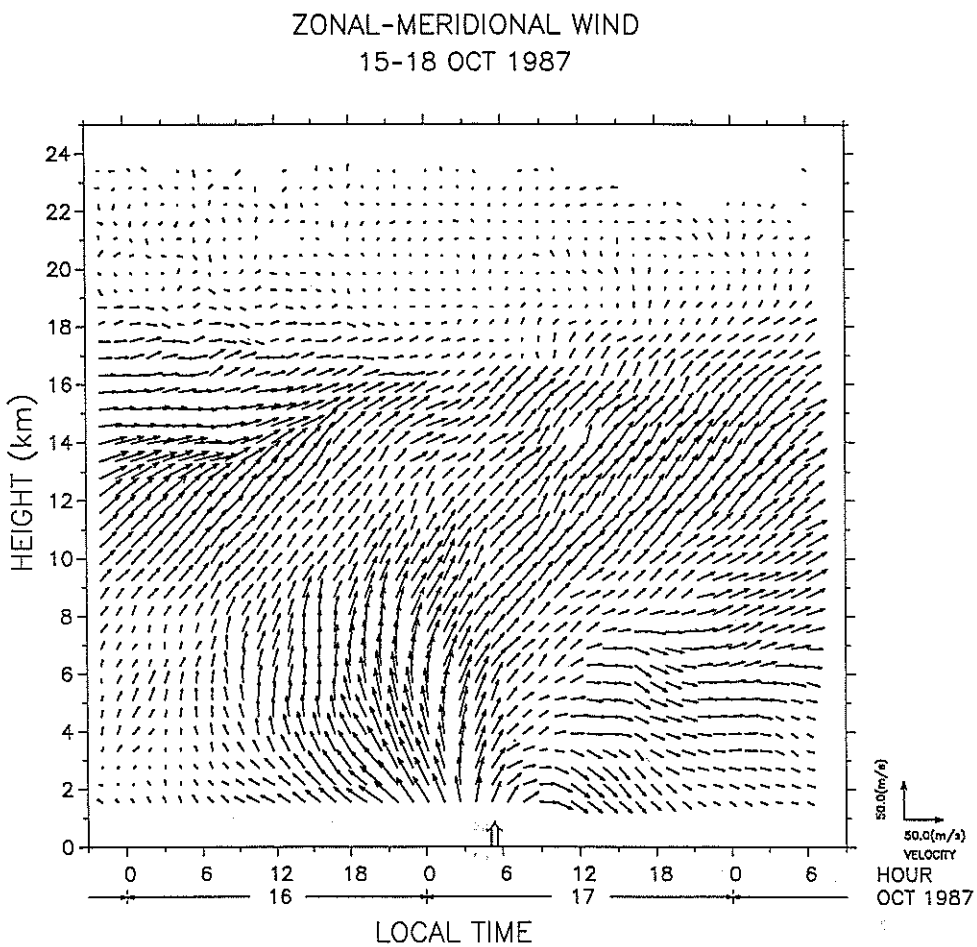

FIG. 2. Time–height variation of the mean horizontal wind. Each arrow denotes the zonal and the meridional wind velocity component averaged over 1 h in time and 600 m in height as a vector with a scale shown on the right of the figure. The thick arrow on the bottom of the figure indicates the passage of the center of the typhoon.

Figures 3a,b shows the fluctuating component of the zonal and the meridional wind component, respectively, around their 60-h mean values at each height. A clear reversal of the zonal wind direction from westward (lighter shades) to eastward (darker shades) is seen in Fig. 3a at the time of storm passage below about 10 km. Above that height, the reversal of the opposite sign (from eastward to westward) takes place, although not as rapidly as at lower heights. The maximum of this counter flow, which is indicative of the outward airflow from the typhoon center at its top, is clearly seen at around 14 km before the passage, but not evident after the passage when the typhoon had already decayed. Most of such bulk motion is limited below the tropopause height of about 16 km, above which wavelike structures with short vertical wavelength of a few kilometers dominate.

Fluctuating components and the mean vertical profile of the vertical wind velocity are given in Fig. 4. One of the important features found in Fig. 4 is the upward flow of about 2 m s^{-1} that continued for about three hours around the time of storm passage at the height range of 8–12 km. Since this height range was already dry at that time, as shown later by the radiosonde data of Fig. 6b, this upward flow seems to be forced lifting above the cloud top. More rapid reversals of upward and downward flows are observed below about 6 km suggesting convective activities.

Downward flows of about -2 m s^{-1} at 2–3 km can be the downdrafts generated by evaporation cooling, although caution should be used because of the possible biases due to contaminations of the echo power spectra by precipitation echoes as described above.

4. Atmospheric stability

The MST radars, including the MU radar, observe echoes from fluctuations in the radio index of refraction mainly caused by atmospheric turbulence in the lower and the middle atmosphere. The echo power is inter-

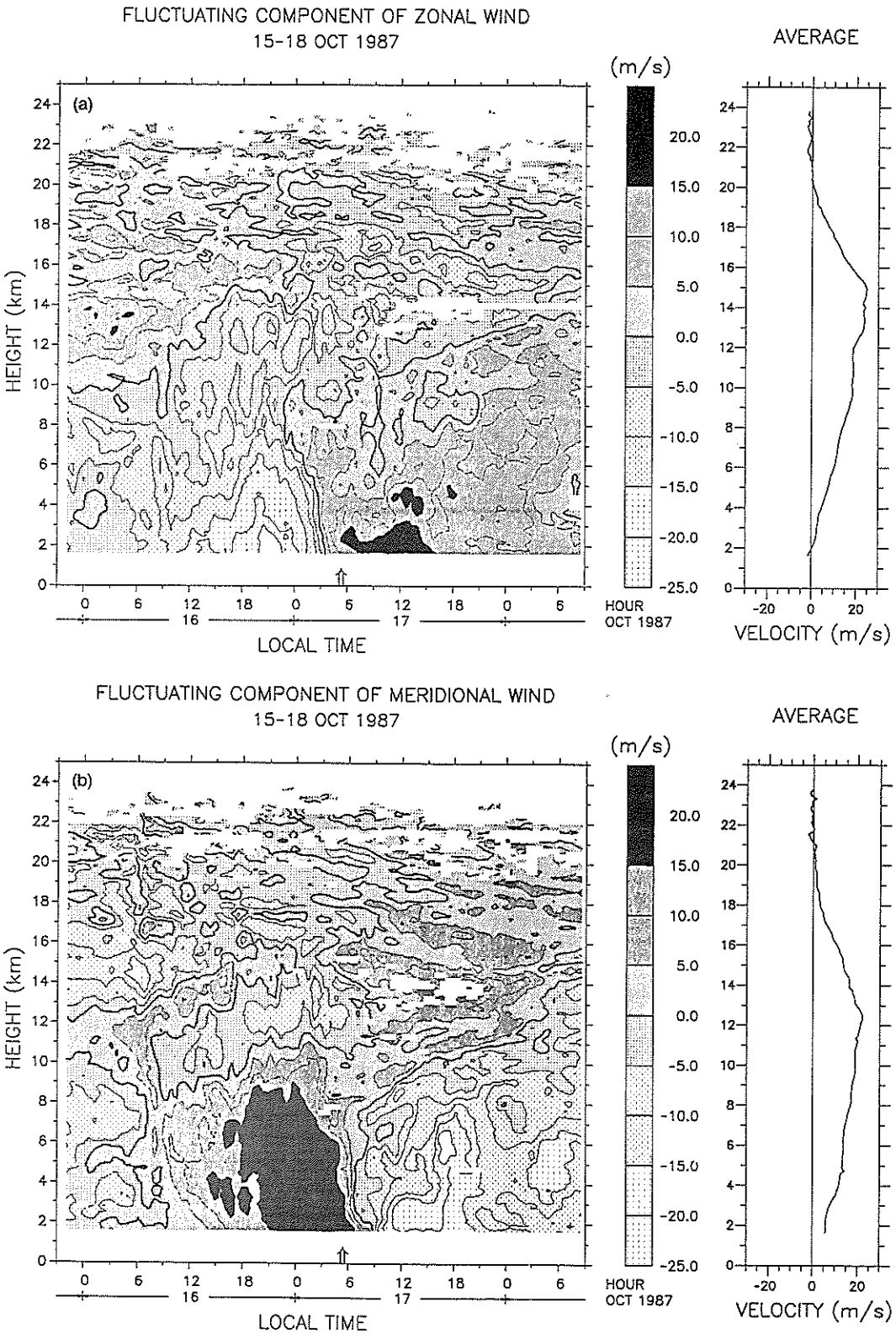

FIG. 3. Fluctuating components of (a) the zonal wind and (b) the meridional wind versus time and height. Contours are drawn from the wind velocity data averaged over 30 min in time. The mean wind profile, which is subtracted from the contour, is shown on the right of each panel. Contours are drawn at an interval of 5 m s^{-1}. The right panel of each figure shows the mean zonal and meridional wind profiles of the whole observation period. Positive values indicate eastward and northward flow, respectively.

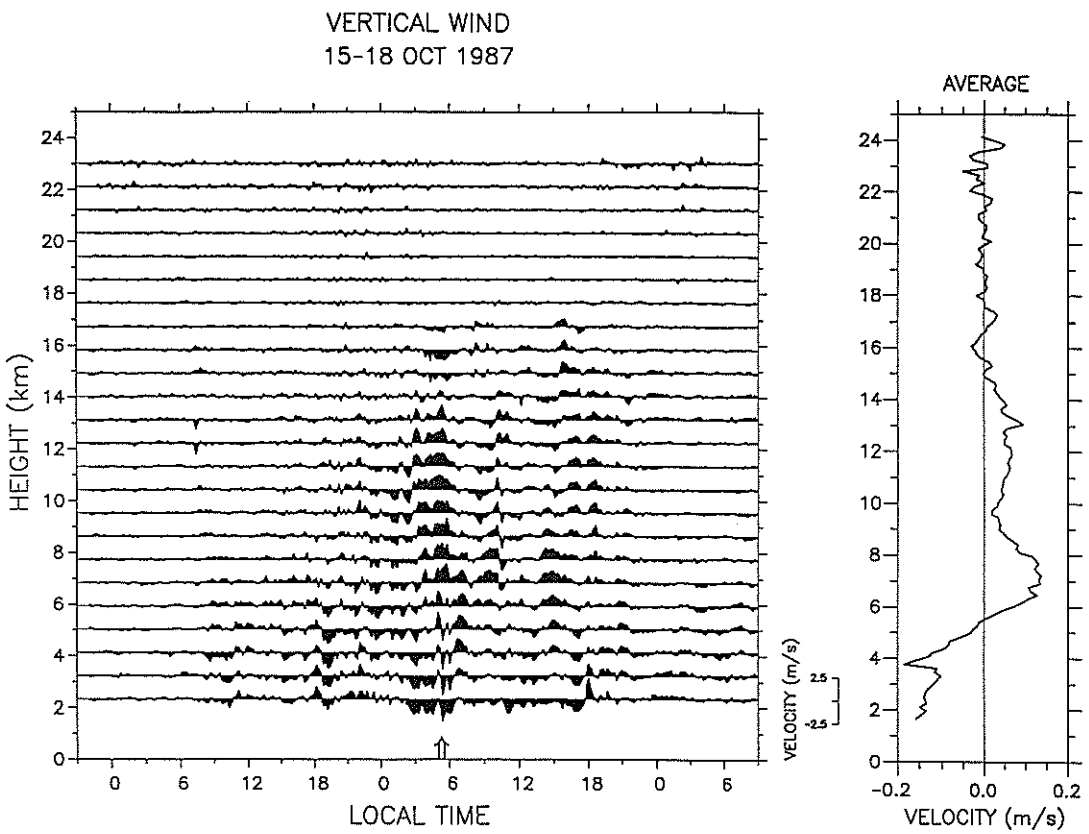

FIG. 4. Fluctuating components of the vertical wind after 10-min low-pass filter. The mean wind profile, which is subtracted from the left panel, is shown on the right.

preted as an index of the magnitude of turbulence weighted by the mean vertical gradient of the index of refraction (e.g. Balsley and Gage 1980).

Figure 5a shows a contour map of the echo power received by the vertically pointing antenna beam versus time and height. The echo power contour is a measure of the activity of atmospheric turbulence, although it is largely affected by the vertical gradient of the index of refraction, which is determined by atmospheric pressure, temperature, and humidity.

A series of nine radiosondes was launched from the MU radar site during the observation period. Figure 6a shows temperature profiles and Fig. 6b shows humidity profiles. The tropopause height and the height of a temperature inversion layer seen at around 8–10 km in the last five launches are determined from Fig. 6a and plotted on Fig. 5a. An abrupt decrease of the humidity is found in the last six humidity profiles shown in Fig. 6b. It starts at 8–9 km about 2 h before the passage.

A strong reflecting layer ascending from 6 to 10 km seen after the passage of the typhoon is obviously associated with some atmospheric discontinuity because its height agrees very well with the height of temperature inversion and also with that of the humidity discontinuity. Considering that the speed of the typhoon was about 10 m s^{-1}, and that the layer lasted over 24 h, the horizontal scale of this layer is estimated to be at least about 1000 km. The temperature inversion is also observed by the radiosonde observations of other stations around the MU radar suggesting this estimate.

The echo power in Fig. 5a also corresponds to another discontinuity of the atmosphere, the tropopause. The tropopause height agrees well with a height where the echo power starts to increase again with height. This correspondence is attributed to the difference in atmospheric stability above and below the tropopause, and has been used to locate the tropopause from the MST radar data (Green and Gage 1980).

Thin turbulence layers produced by local dynamic instabilities caused mainly by gravity waves in a stably stratified atmosphere cause the aspect-sensitive scattering or specular reflection. It is characterized by an enhanced echo power observed by the vertically pointing beam over that observed from other directions (Gage and Green 1978). Figure 5b shows the ratio of the echo power by the vertical beam to the echo power observed by a beam pointing to 10° from the zenith toward the east. The ratio of the echo power of the vertical direction to an oblique direction can therefore

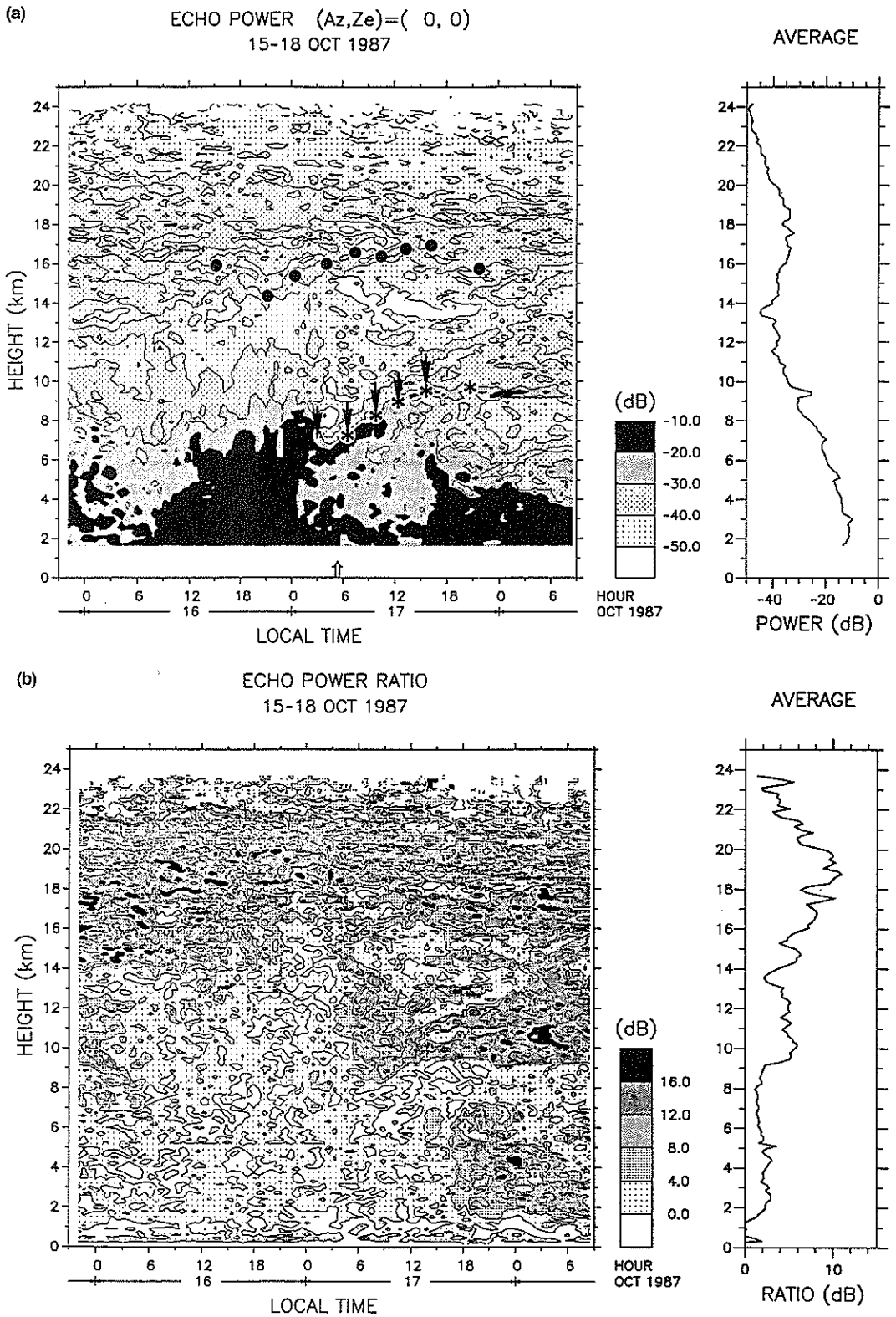

FIG. 5. (a) The observed echo power in the vertical direction. (b) The ratio of the echo power in the vertical direction to the echo power in an oblique direction with 10° off-zenith angle. Contours are drawn at an interval of 10 dB in an arbitrary unit. The right panel shows the mean echo power profile. Circular marks in (a) denote the tropopause height as determined from the temperature profiles shown in Fig. 6a. Asterisks indicate the height of a temperature inversion in the troposphere seen in Fig. 6a. Arrow heads indicate the cloud-top height as derived from Fig. 6b. Humidity above about 12 km, where the temperature is less than −40°C, is not reliable.

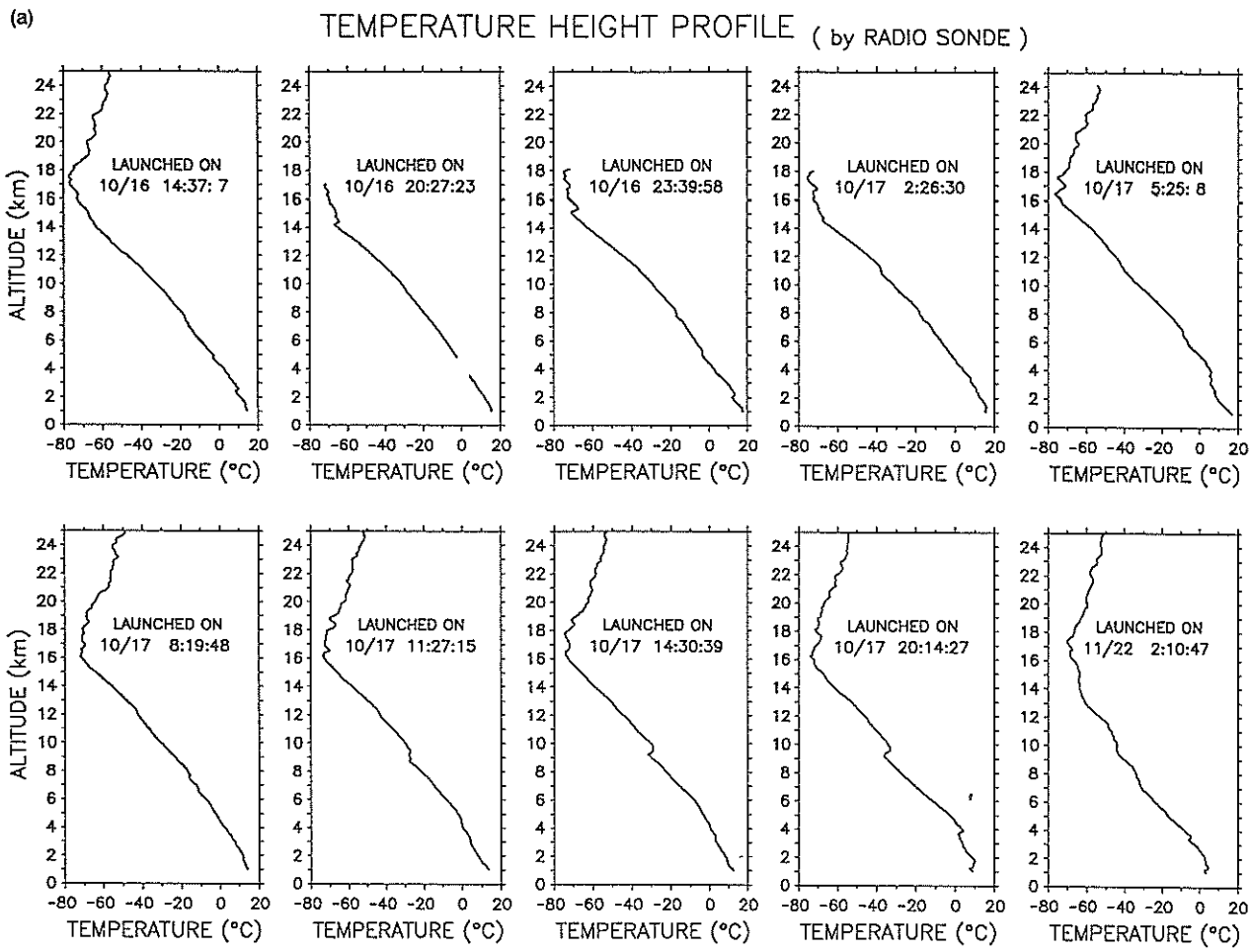

FIG. 6. (a) Temperature and (b) relative humidity versus height obtained by nine radiosondes launched from the MU radar site during the observation. The time of launch is in JST (same as other figures).

be used as an index of stability of the background atmosphere (Fukao et al. 1986). While isotropic scattering suggests that the medium is convectively unstable or at least has a low-stability, high-aspect sensitivity usually means a thin turbulence layer in a stable background condition.

From Fig. 5b, the enhancement of the vertical power is evident in two regions: 1) above tropopause height, and 2) above the height of temperature inversion after the passage of the typhoon. The vertical velocity is very small in the second region as shown in Fig. 4, which is consistent with the stability of the background air expected from the enhanced echo power ratio. This height region shows a clear contrast before and after the passage of the typhoon. Before the passage, it is characterized by a high humidity as shown by the first three panels of Fig. 6b and a low stability. The same height region drastically changes its characteristics into a dry and vertically stable condition. This is a good example of discontinuity between the air masses surrounding a typhoon.

5. Long-period waves

In the decaying stage of a typhoon it is anticipated that an appreciable part of the energy associated with the typhoon is released in a form of gravity waves. MST radar observations of typhoons have indeed detected large variability due to gravity waves in the wind field (Kato et al. 1984; Hung et al. 1988). Detection of an internal gravity wave associated with a typhoon by the network of surface pressure measurements is also reported (Matsumoto and Okamura 1985).

The present observations are suited for studying gravity waves since the wind vector was monitored at 2.5-min and 150-m intervals in time and height, respectively, covering the entire frequency spectrum ranging from the Brunt–Väisälä period to the inertial period. Since details of the observed gravity waves are reported elsewhere (Sato 1991a,b), an example of the pronounced waves are presented here.

In Fig. 3, downward phase progression can be seen above about 16 km. It is characterized by fairly short

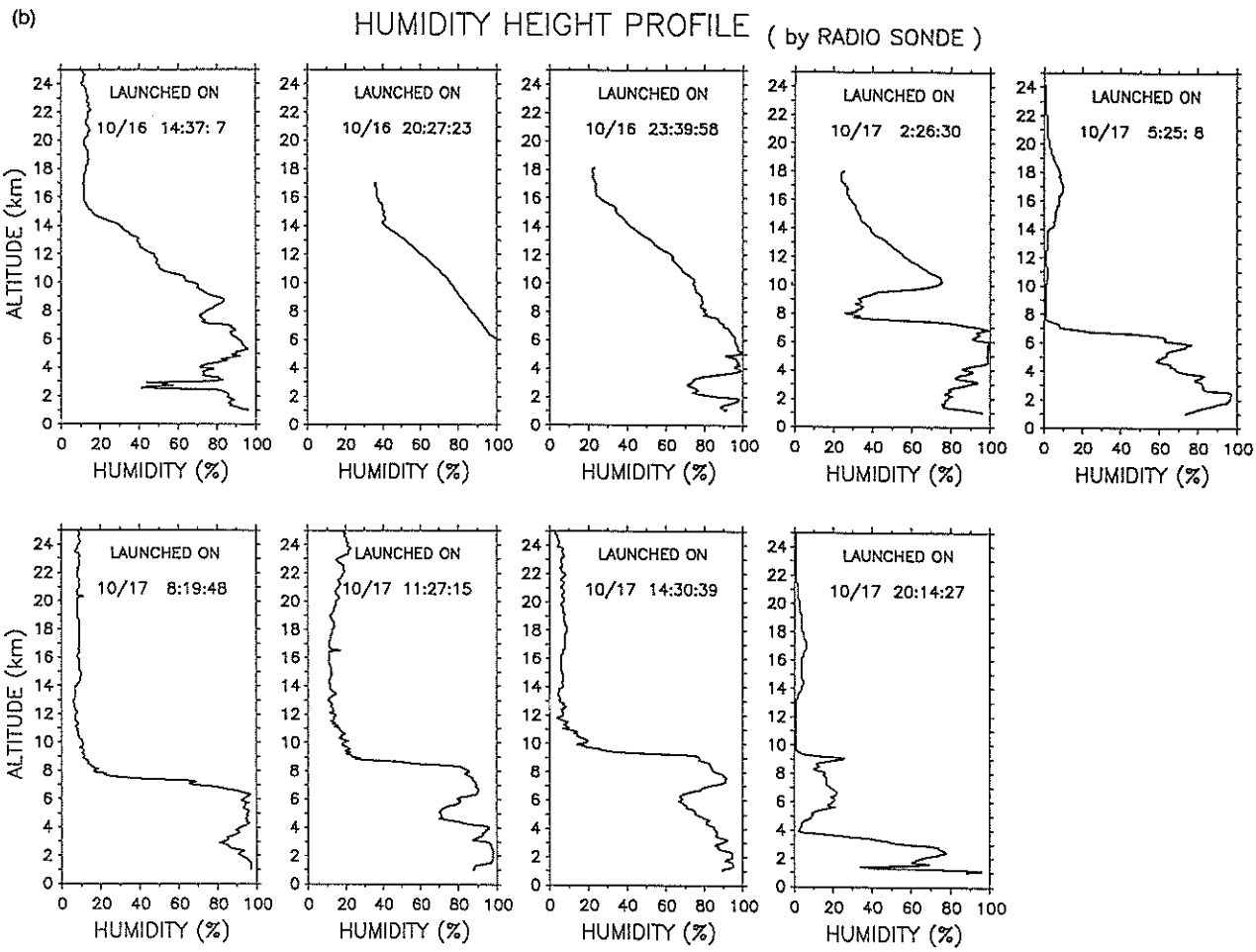

FIG. 6. (*Continued*)

(2–4 km) vertical wavelengths and apparent periods of the order of 10 h. Figure 7 shows a filtered zonal wind component with vertical filter response centered at wavelengths of 1.5–4.5 km versus time and height.

While no clear phase progression is observed before the passage of the typhoon, a remarkable tendency of upward and downward phase progression below and above about 14 km, respectively, appears after the passage. A similar result is obtained also for the meridional wind component. Although this apparent phase progression suggests the generation of inertia-gravity waves at that height, it can be affected by the Doppler shifting of the waves due to the mean flow.

In order to avoid this problem, the vertical propagation of these waves was checked by a hodograph analysis introduced by Hirota and Niki (1985) that makes use of the rotation of the wind vector in the horizontal plane versus height to determine the vertical propagation characteristics of the wave at each time. This method is free from the Doppler effect because it uses a snapshot of the wave that does not contain any information on its change in time. Figure 8 gives an example of the hodograph. This figure shows the change of the wind vector with height in a height range of 7.8–14 km after one hour of averaging in time and a bandpass filtering of 1.5–4.5 km in height in order to remove other waves and fluctuations. The trace shows a counterclockwise rotation as the height increases from 7.8 until 9.5 km, reverses the direction of rotation until 13 km, then reverses again above that height, indicating the dominance of three types of waves at different height regions.

The intrinsic period of the wave relative to the inertial period (21 h) is given by the ratio of the minor axis to the major axis of the ellipse. The direction of propagation is along the major axis and its sign is determined by the phase relation between the horizontal and vertical velocity components. For example, the intrinsic period around the height of 12 km determined is 11–13 h. The wave is propagating toward south-southwest, which is away from the typhoon center. The intrinsic period of the wave in the lower region below 9.5 km is about 5 h, while it is larger than 15 h in the upper region above 13 km. It should be noted that this

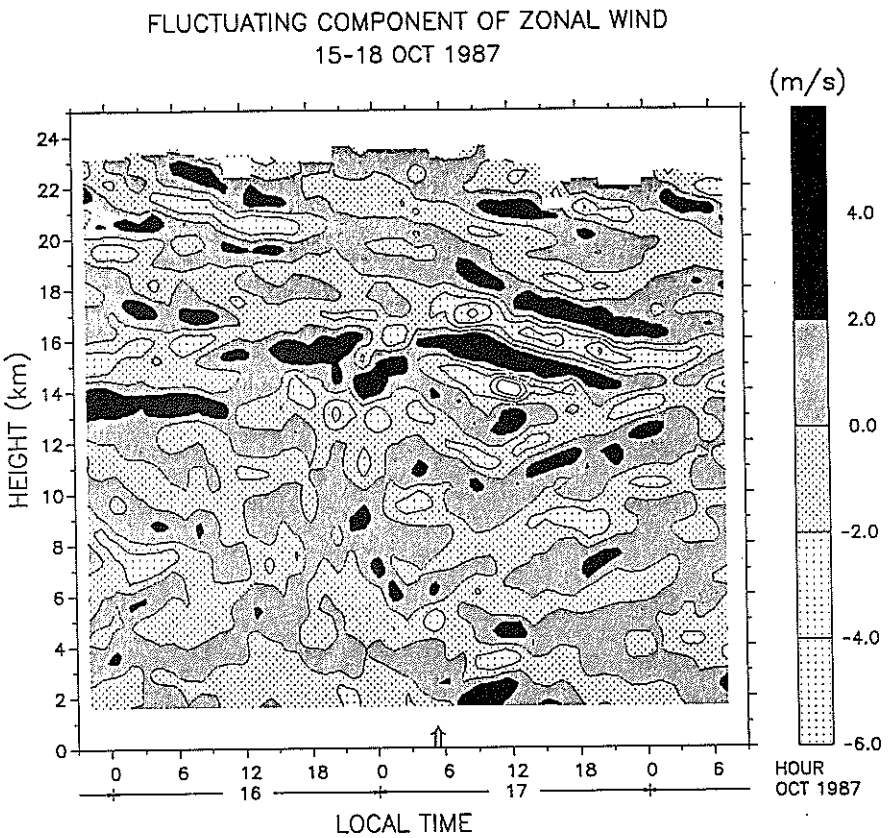

FIG. 7. Zonal wind component as shown in Fig. 3, but with vertical wavelengths of 2–4 km. Contours are drawn every 2 m s^{-1} and darker shade denotes eastward components.

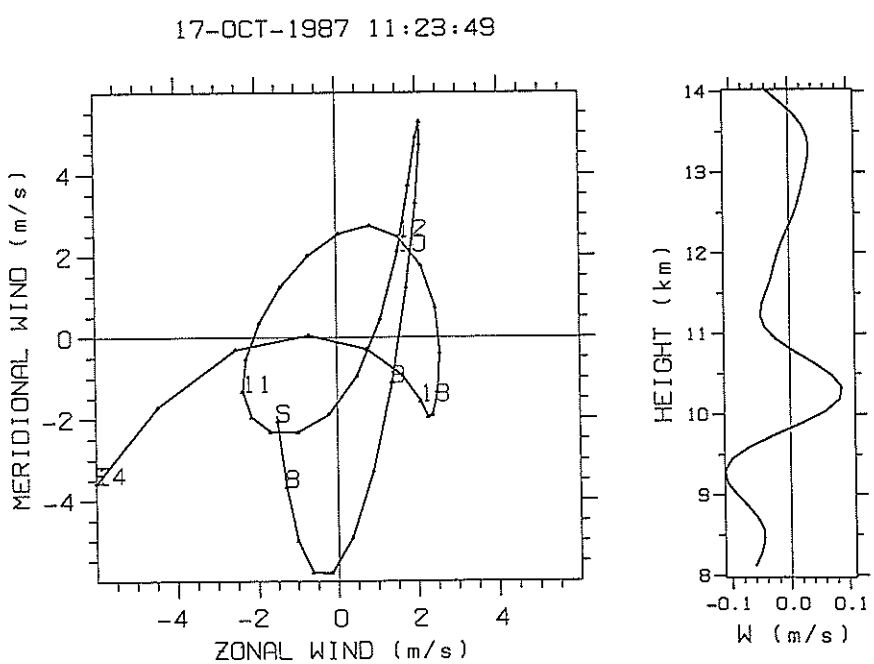

FIG. 8. An example of the hodograph of the horizontal wind. A trace of the wind vector versus height is drawn in a height range of 7.8–14 km after one hour of averaging in time and a band-pass filtering of 1.5–4.5 km in height.

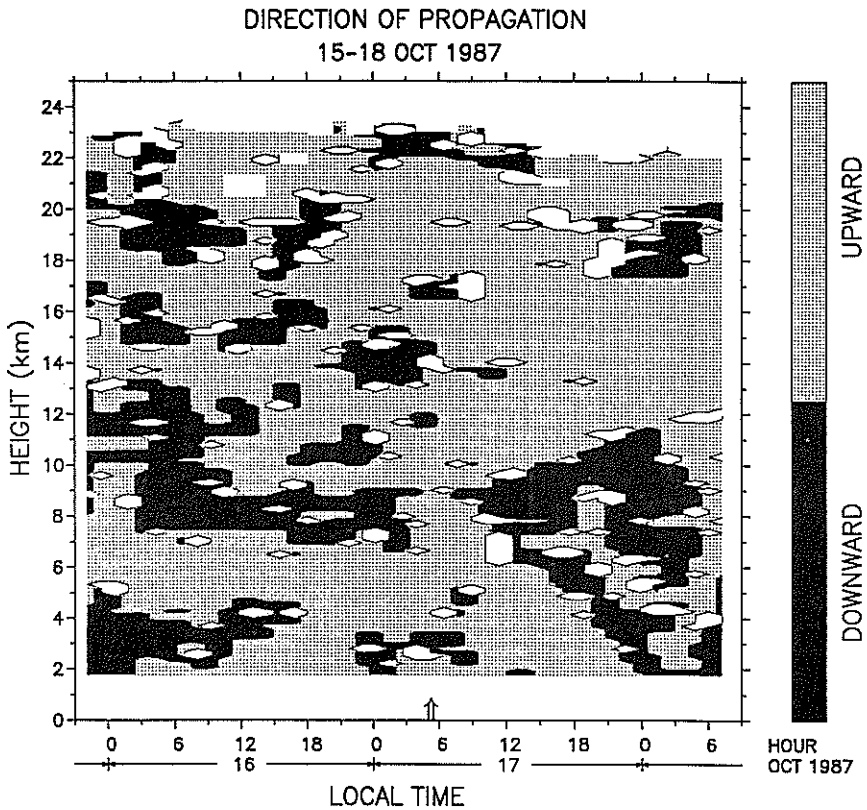

FIG. 9. Direction of vertical propagation of the waves shown in Fig. 7 as determined by the hodograph analysis.

type of analysis assumes that there is a single wave at a given height, and thus is valid only when such a condition is satisfied. Although this condition is not fully satisfied in the present case, dominance of a single wave at each height is evident by the linear structure of the contours in Fig. 7.

Considering the relatively short vertical wavelength and the large variability of the wave characteristics with height, it is not always easy to determine the wave characteristics at each time and height. Instead, it is determined whether the wave is propagating upward or downward at each height. It is judged by inspecting the trace of the horizontal wind velocity vector at the two adjacent heights around the height of concern and by determining whether the hodograph has a right-hand or a left-hand curvature with height.

Figure 9 indicates by the shading the portion of the waves propagating upward and downward in the time–height section as Fig. 3. The dark and light shades denote downward and upward propagation, respectively. The predominance of upward propagation seems to indicate the general tendency of upward energy transport by gravity waves. An outstanding feature of this figure is a clear reversal of propagation direction starting from 0700 JST on 17 October at about the 9-km height. The boundary between downward and upward propagation ascends linearly with time and reaches 12 km after about 19 h. Existence of regions with clear downward and upward propagation below and above this boundary, respectively, suggests the generation of these waves here.

It should be noted that the location of the strong scattering layer accompanied by a temperature inversion discussed in the previous section agrees with the upper boundary of downward propagation. Since the layer obviously indicates a discontinuity in the atmosphere, where a large amount of energy associated with the typhoon is consumed, it is most likely to be the source of the wave activity discussed here.

6. Short-period waves and oscillations

In addition to such long period waves, a substantial amplitude was observed for much shorter-period components of the wind fluctuations. The high-frequency components of the gravity waves are, in general, harder to identify than the longer-period waves because of their larger spatial variability and larger Doppler shifts due to shorter horizontal wavelengths. Here only the total activity is examined through their amplitude rather than inspecting the individual wave components.

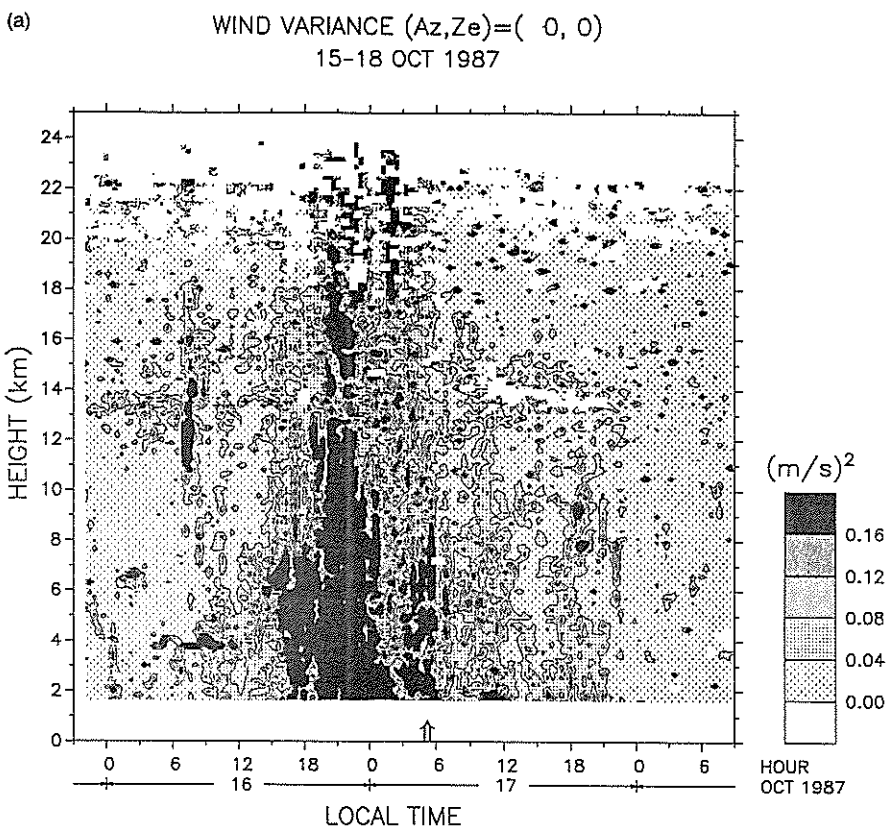

FIG. 10. Variance of the vertical wind fluctuations with periods of less than 20 min in time and with (a) no vertical filtering and (b) a high-pass filter with the cutoff wavelength of 4.5 km in height.

Figure 10a shows the variance of the vertical wind fluctuations with periods of less than 20 min versus height and time. It is calculated by taking the square of the vertical wind velocity after applying a high-pass filter with the cutoff period of 20 min to the velocity time series at each height. These short-period fluctuations are more directly related to the disturbances associated with the typhoon, including the convective motion and the short period gravity waves generated locally.

Although the temporal growth and decay of the activity is readily explained by the convection inside the typhoon, it is surprising that the enhanced activity in the fluctuations reaches to the maximum observed height of 24 km, which is much higher than the top of the typhoon as indicated in Figs. 2 or 3. The characteristics of such disturbances can be examined from their vertical structures. Figure 10b shows the same amplitude of fluctuations as Fig. 10a, but of only those components with vertical wavelengths less than 4.5 km. Comparison between Figs. 10a,b shows that most of the fluctuations that reach above 10 km have very large (>4.5 km), if not infinite, vertical wavelengths typical of the evanescent modes. These fluctuations are likely to be the free oscillation with the Brunt–Väisälä period excited by the convective motion within the typhoon or the waves close to that period.

In contrast to the free oscillation-like behavior of the short-period disturbances at higher altitudes, fluctuations in the lower troposphere contain shorter vertical-wavelength components as well. They can include convective motion itself as well as the propagating internal gravity waves. Even when convective motion have a fairly long time constant of 20–30 min, it is observed by a fixed observer as fluctuations with shorter period in the presence of mean wind because the horizontal size of convective cells in the lower troposphere is usually small. Since the internal gravity wave components with high intrinsic frequencies have larger dissipation rates than the long-period waves, it is reasonable that they are also confined to the vicinity of their plausible source of the convective cells and the surface boundary layer.

7. Summary

Basic results have been presented with a few interesting examples among various phenomena found in a series of observation of a typhoon made with the MU radar. Besides the importance of measuring the full

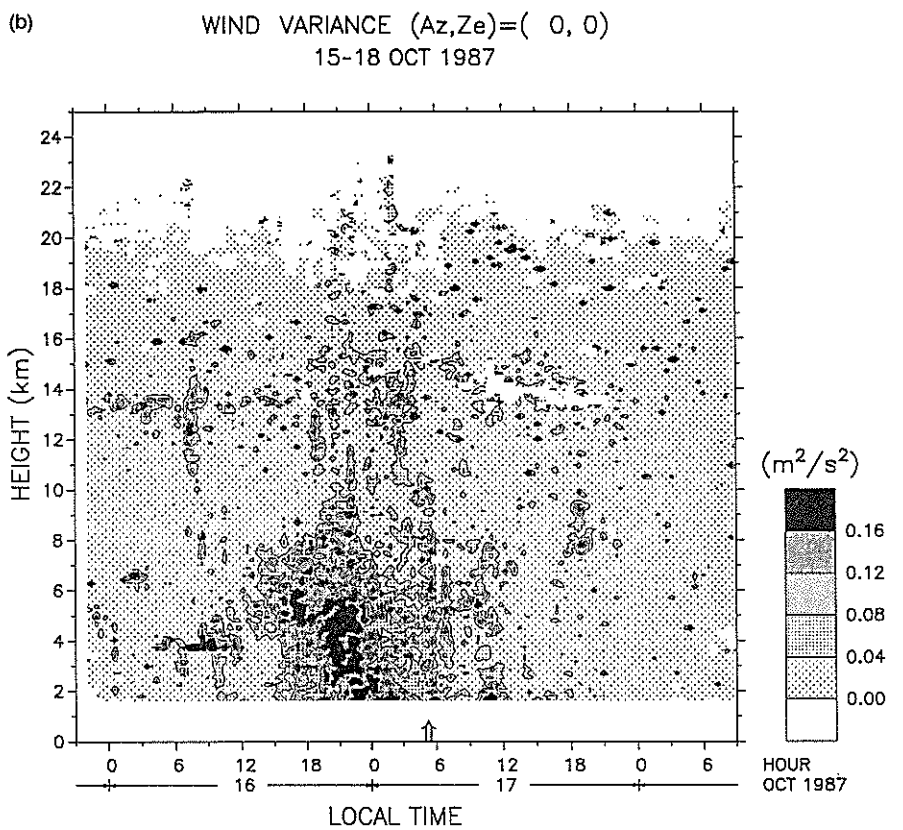

FIG. 10. (*Continued*)

vertical structure of a typhoon with the MST radar technique for the first time, the observation has shown the existence of various waves associated with the typhoon. Although the analyses are yet rather preliminary, they have shown a clear correspondence of the waves with their sources, which is one major advantage of studying isolated disturbances such as a typhoon.

Acknowledgments. Special thanks are due Kaoru Sato for her valuable suggestions and discussion. Comments by reviewers were very helpful for improving the manuscript.

The MU radar belongs to and is operated by the Radio Atmospheric Science Center of Kyoto University.

REFERENCES

Balsley, B. B., and K. S. Gage, 1980: The MST radar technique: Potential for middle atmospheric studies. *Pure Appl. Geophys.*, **118,** 452–493.

Chao, J. K., F. S. Kuo, Y. S. Chu, I. J. Fu, J. Röttger and C. H. Liu, 1986: The first operation and results of the Chung-Li VHF radar. *Handbook for MAP,* **20,** 359–363.

Franklin, J. L., J. L. Lord and F. D. Marks, 1988: Dropwindsonde and radar observations of the eye of Hurricane Gloria (1985). *Mon. Wea. Rev.*, **116,** 1237–1244.

Fukao, S., T. Sato, T. Tsuda, S. Kato, K. Wakasugi and T. Makihira, 1985a: The MU radar with an active phased array system: Part I: Antenna and power amplifiers. *Radio Sci.*, **20,** 1155–1168.

——, T. Tsuda, T. Sato, S. Kato, K. Wakasugi and T. Makihira, 1985b: The MU radar with an active phased array system: Part II: Inhouse equipment. *Radio Sci.*, **20,** 1169–1176.

——, T. Sato, T. Tsuda, M. Yamamoto and S. Kato. 1986: High-resolution turbulence observations in the middle and lower atmosphere by the MU radar with fast beam steerability: Preliminary results. *J. Atmos. Terr. Phys.*, **48,** 1269–1278.

Gage, K. S., and J. L. Green, 1978: Evidence for specular reflection from monostatic VHF radar observations of the stratosphere. *Radio Sci.*, **13,** 991–1001.

Green, J. L., and K. S. Gage, 1980: Observations of stable layers in the troposphere and stratosphere using VHF radar. *Radio Sci.*, **15,** 395–405.

Hirota, I., and T. Niki, 1985: A statistical study of inertia-gravity waves in the middle atmosphere. *J. Meteor. Soc. Japan,* **63,** 1055–1066.

Hung, R. J., Y. D. Tsao, D. L. Johnson, A. J. Chen, C. H. Lin, J. M. Cheng and C. M. You, 1988: VHF radar remote sensing of atmospheric parameters over Taiwan during the time period of typhoon Wayne. *Int. J. Remote Sensing,* **9,** 477–493.

Ishihara, M., Z. Yanagisawa, H. Sakakibara, K. Matsuura and J. Aoyagi, 1986: Structure of a typhoon rainband observed by two Doppler radars. *J. Meteor. Soc. Japan,* **64,** 923–939.

Jorgensen, D. P., 1984a: Mesoscale and convective-scale characteristics of mature hurricanes. Part I: General observations by research aircraft. *J. Atmos. Sci.*, **41,** 1268–1285.

——, 1984b: Mesoscale and convective-scale characteristics of mature hurricanes. Part II: Inner core structure of Hurricane Allen (1980). *J. Atmos. Sci.*, **41,** 1287–1311.

——, E. J. Zipser and M. A. LeMone, 1985: Vertical motions in intense hurricanes. *J. Atmos. Sci.*, **42**, 839–856.

Kato, S., T. Ogawa, T. Tsuda, T. Sato, I. Kimura and S. Fukao, 1984: The middle and upper atmosphere radar: First results using a partial system. *Radio. Sci.*, **19**, 1475–1484.

Larsen, M. F., and J. Röttger, 1982: VHF and UHF Doppler radars as tools for synoptic research. *Bull. Amer. Meteor. Soc.*, **63**, 996–1008.

Marks, F. D., and R. A. Houze, 1984: Airborne Doppler radar observations in Hurricane Debby. *Bull. Amer. Meteor. Soc.*, **65**, 569–582.

——, and ——, 1987: Inner core structure of Hurricane Alicia from airborne Doppler radar observations. *J. Atmos. Sci.*, **44**, 1296–1317.

Matsumoto, S., and H. Okamura, 1985: The internal gravity wave observed in the Typhoon T8124 (Gay). *J. Meteor. Soc. Japan*, **63**, 37–51.

Sakakibara, H., M. Ishihara and Z. Yanagisawa, 1985: Structure of a typhoon rainstorm in the middle latitudes observed by Doppler radar. *J. Meteor. Soc. Japan*, **63**, 901–922.

Sato, K., 1991a: Wind disturbances associated with Typhoon 8719 observed with the MU radar. Part I: Difference between before and after the typhoon passage. *J. Atmos. Sci.*, submitted.

——, 1991b: Wind disturbances associated with Typhoon 8719 observed with the MU radar. Part II. Detailed characteristics and effects on the typhoon. *J. Atmos. Sci.*, submitted.

Sato, T., H. Doji, H. Iwai, I. Kimura, S. Fukao, M. Yamamoto, T. Tsuda and S. Kato, 1990: Computer processing for drop-size distributions and vertical air velocities from VHF Doppler radar spectra. *Radio Sci.*, **25**, 961–973.

Weatherford, C. L., and W. M. Gray, 1988a: Typhoon structure as revealed by aircraft reconnaissance. Part I: Data analysis and climatology. *Mon. Wea. Rev.*, **116**, 1032–1043.

——, and ——, 1988b: Typhoon structure as revealed by aircraft reconnaissance. Part II: Structural variability. *Mon. Wea. Rev.*, **116**, 1044–1056.

Yamamoto, M., T. Sato, P. T. May, T. Tsuda, S. Fukao and S. Kato, 1988: Estimation error of spectral parameters of mesosphere–stratosphere–troposphere radars obtained by least squares fitting method and its lower bound. *Radio Sci.*, **23**, 1013–1021.